The impact of atmospheric dynamics on vertical cloud overlap over the Tibetan Plateau

Jiming Li[1,*], Qiaoyi Lv[2], Bida Jian[1], Min Zhang[1],
Chuanfeng Zhao[3], Qiang Fu[1, 4], and Kazuaki Kawamoto[5], Hua Zhang[6]

[1]Key Laboratory for Semi-Arid Climate Change of the Ministry of Education, College of Atmospheric Sciences, Lanzhou University, Lanzhou, China
[2]Laboratory of Straits Meteorology, Xiamen Meteorological Bureau, Xiamen, China
[3]State Key Laboratory of Earth Surface Processes and Resource Ecology, and College of Global Change and Earth System Science, Beijing Normal University, Beijing, China
[4]Department of Atmospheric Sciences, University of Washington, Seattle, USA
[5]Graduate School of Fisheries and Environmental Sciences, Nagasaki University, Nagasaki, Japan
[6]Laboratory for Climate Studies, National Climate Center, China Meteorological Administration, Beijing, China

Corresponding author: Jiming Li, Key Laboratory for Semi-Arid Climate Change of the Ministry of Education, College of Atmospheric Sciences, Lanzhou University, Lanzhou, Gansu 730000, China. (lijiming@lzu.edu.cn)

Abstract

The accurate representation of cloud vertical overlap in atmospheric models is particularly significant for predicting the total cloud cover and for the calculations related to the radiative budget in these models. However, it has received too little attention due to the limited observation, especially over the Tibetan Plateau (TP). In this study, 4 years (2007–2010) of data from the CloudSat cloud product and collocated ERA-Interim reanalysis product were analyzed to examine the monthly and zonal variations of cloud overlap properties over the TP region, and evaluate the effect of atmospheric dynamics on cloud overlap.

Unique characteristics of cloud overlap over the TP have been found. The statistical

results verify that continuous cloud layers tend to maximum overlap at small distance but gradually randomly overlapped with increasing of layer distance. Focusing on the continuous cloud layers, we find that overlap parameter is sensitivity to the unique thermo-dynamical environment of the TP. That is, the unstable atmospheric stratification and correspondingly weak wind shear over the TP lead to greater α values, which is well agreement with the results reported in previous studies. Finally, by using multiple linear regression method, we parameterize decorrelation length scale *L* as a function of the wind shear and atmospheric stability. Compared with other parameterizations, this new scheme improves the prediction of cloud cover over TP when cloud layers distances are above 1km. These results thus indicate that effects of wind shear and atmospheric stability on cloud overlap should both be taken into account in the parameterization of overlap parameter α to improve the simulation of total cloud cover in models.

1. Introduction

Clouds can cause considerable changes in the Earth's radiation budget, the global hydrological cycle and large-scale atmospheric circulations via changes in their various macrophysical (e.g., cloud cover, height, and thickness) and microphysical properties (e.g., cloud phase and droplet and crystal size) (Rossow and Lacis, 1990; Hartmann et al., 1992; Stephens, 2005; Kawamoto and Suzuki, 2012; Yan et al., 2012; Wang et al., 2010). However, our incomplete understanding of their underlying physical processes makes the representation of clouds in climate models still unreliable, which keeps clouds as the largest uncertainty when estimating and interpreting changes in the Earth's energy budget (Boucher et al., 2013).

The Tibetan Plateau (TP), which is also known as the "roof of the world" or the "world water tower", plays a significant role in determining global atmospheric circulations, in addition to its strong influence over Asia via its thermal and dynamic forcings (Yanai et al., 1992; Ye and Wu, 1998; Duan and Wu, 2005; Xu et al., 2008; Wu et al., 2015). Specifically, the TP has experienced distinct climate changes over the past three decades (Kang et al., 2010) that have changed its atmospheric and hydrological cycles (Yang et al., 2014). For example, many studies have showed that significant warming occurs in the TP region during the last decades and will continue to warm in the

future (e.g., Duan et al., 2006; Wang et al., 2008). The rapid warming has caused glacier retreat and expansion of glacier-fed lakes (Zhu et al., 2010), permafrost degradation and temperature increasing (Cheng and Wu, 2007), heating source became weakened (Yang et al., 2011) and corresponding variation of summer precipitation downstream (Duan et al., 2013). In addition to increased greenhouse gas emission, Kang et al. (2010) summarized that the changes of cloud cover also is one of dominant factors causing the rapid warming over TP region. Indeed, some studies have linked the rapid warming to variations in the cloud cover over the TP region (e.g., Chen and Liu, 2005; Duan and Wu, 2006; Li et al., 2006; Yang et al., 2012; You et al., 2014; Wu et al., 2014). Such as, a recent study has indicated that increased nocturnal cloud cover over the northern TP would increase the nighttime temperature by enhanced atmospheric back-radiation, while decreased daytime cloud over the southern TP has contributed to the increasing of surface air temperature during daytime(Duan and Xiao, 2015). Based on the above studies, it is necessary to reasonably simulate the cloud cover in the climate models in order to better predictions these climate changes over TP.

However, our understanding about the role of cloud cover on the radiation balance and water cycle over the TP region remains poor because of the limited availability of regional cloud observations and our incomplete knowledge of the cloud physical processes for use in weather forecasting and climate models. One of the remaining challenges involves how to reasonably represent the characteristics of the vertical overlapping of cloud layers in these models. The different cloud overlap parameterizations (e.g., whether it is at a maximum, minimum or random assumptions) used in the models may result in distinctly different total cloud covers. The maximum assumption minimizes the total cloud cover, while minimum assumption produces minimally overlap between cloud layers and results in maximum total cloud cover. The total cloud cover predicted by the random assumption will fall somewhere between maximum and minimum assumptions. For example, if the cloud covers in two model layers are given as 50%, then the maximum overlap will result in a total cloud cover of 50%, and a minimum overlap will result in an overcast condition (a complete cloud cover, i.e., 100%). The differences between the predicted total cloud covers will also significantly affect the calculated radiative budgets and heating/cooling rate profiles in

the model simulations (Morcrette and Fouquart, 1986; Barker et al., 1999; Chen et al., 2000; Pincus et al., 2005; Zhang et al., 2013a; 2013b; 2016; Jing et al., 2016). Previously published general circulation model (GCM) simulation results have indicated that the bias in the global mean radiation fluxes at the top of the atmosphere and at the surface, which is caused by the different overlap conditions only, can reach 20-40 W m^{-2} (Morcrette and Jakob, 2000; Jing et al., 2009; Zhang and Jing, 2010).

Ground-based radar observations can be used to improve the cloud overlap assumptions in the models because radar signals produce relatively reliable cloud mask profiles (e.g., Hogan and Illingworth, 2000; Mace and Benson-Troth, 2002; Willén et al., 2005; Naud et al., 2008; Oreopoulos and Norris, 2011) than other passive measurements. However, these observations are only one-dimensional, and the radar sites are very sparsely distributed, especially in the TP region. Passive sensors and traditional surface weather reports fail to detect vertical cloud structures, and only providing limited information about the cloud overlap (Chang and Li, 2005a, b; Huang, 2006; Huang et al., 2005, 2006a). Therefore, an active space-based radar measurement is the best choice for identifying the vertical overlap properties of clouds and thereby, better quantifying the radiative budget at the surface and its related climate change impacts (e.g., glacier degradation and frozen soil ablation) over the TP region.

Fortunately, the millimeter-wavelength cloud profiling radar (CPR) launched on CloudSat (Stephens et al., 2002) and the cloud-aerosol lidar with orthogonal polarization (CALIOP) (Winker et al., 2007) launched on CALIPSO (Cloud-Aerosol Lidar and Infrared Pathfinder Satellite Observation) provide an unprecedented opportunity to investigate vertical cloud overlaps on a global scale (Barker et al., 2008; Kato et al., 2010; Li et al., 2011; 2015; Tompkins and Di Giuseppe, 2015; Di Giuseppe and Tompkins, 2015). Based on two months of cloud mask profile information from the CloudSat and CALIPSO satellites, Barker (2008) quantified the properties of cloud overlap on a global scale and identified a latitudinal dependence. Recently, Di Giuseppe and Tompkins (2015) further evaluated the impact of wind shear on the global-scale cloud overlap and identified an empirical relationship between the cloud overlap and wind shear for use in models by using 6 months of CloudSat-CALIPSO data. However, the related question of the cloud overlapping over the TP region has received too little attention, as has the

question of how the unique thermo-dynamical environment (e.g., the atmospheric stability) of the TP region affects cloud overlap. As such, this study mainly focuses on the impacts of various atmospheric states and large-scale atmospheric dynamics on cloud overlap over the TP region by combining the cloud cover profile information from the 2B-GEOPROF-LIDAR dataset (Mace et al., 2009) and the meteorological parameters from the ERA-Interim reanalysis datasets (Dee et al., 2011).

This paper is organized as follows: a brief introduction to all the datasets and methods used in this study is given in Section. 2. Section 3.1 outlines the monthly and zonal variations of the cloud overlap parameters over the TP region. Further analyses of the impacts of the variations in the atmospheric state and large-scale atmospheric dynamics on cloud overlap are provided in Sections. 3.2. Finally, the conclusions and discussion are presented in Section. 4.

2. Datasets and methodology

In this study, 4 years (2007–2010) of data from CloudSat 2B-GEOPROF-LIDAR, ECMWF-AUX and the daily 6-hour ERA-Interim reanalysis were collected to analyze the impacts of atmospheric dynamics on the cloud overlap over the TP (27 °N-39 °N;78 °E-103 °E) region as demonstrated in Fig. 1a.

2.1 Satellite datasets

Radar signals can penetrate the optically thick layers that attenuate lidar signals significantly, and lidar signals may sense the optically thin hydrometeor layers that are below the detection threshold of radar signals. Thus, by combining the unique complementary capabilities of the CPR on CloudSat and the space-based polarization lidar (CALIOP) on the CALIPSO satellite, the 2B-GEOPROF-LIDAR dataset can produce the most accurate quantitative descriptions of the locations of the hydrometeor layers in the atmosphere on the global scale (Mace and Zhang, 2014). In the dataset, every CloudSat profile includes 125 height layers (e.g., vertical bin), and the "*CloudFraction*" parameter reports the fraction of the lidar volume within each radar vertical bin that contains hydrometeors (Mace et al., 2009; Mace and Zhang, 2014). Several previous studies have identified a cloudy atmospheric bin based on different thresholds of the lidar-identified cloud fraction, including a 99% (Barker, 2008; Di Giuseppe and Tompkins, 2015) or 50% threshold (Haladay and Stephens, 2009;

Verlinden et al., 2011). Here, a threshold of 99% is used in our study. However, due to the significant attenuation of lidar signals to the optically thick layers, this parameter fails to provide the "*CloudFraction*" value in those optically thick layers. Thus, we have to use other radar information (that is, cloud "*LayerBase*" and "*LayerTop*" fields) from the aforementioned dataset as supplementary to construct the complete two-dimensional cloud mask (See Fig. 1b). In addition, the ECMWF-AUX dataset (Partain, 2004), which is an intermediate dataset that contains the set of ancillary ECMWF state variable data interpolated across each CloudSat CPR bin, are also used to provide the pressure and height information of each vertical bin in the cloud mask profile. The vertical and horizontal resolutions of these products are 240 m and 1.1 km, respectively.

2.2 Meteorological reanalysis dataset

The daily 6-hourly dataset from the ERA-Interim reanalysis (Dee et al., 2011), which has a grid resolution of $0.25°\times0.25°$, is used to characterize the atmospheric dynamics over the TP. For each cloud mask profile in the 2B-GEOPROF-LIDAR dataset, the vertical profiles of the zonal wind *u*, meridional wind *v*, relative humidity *rh*, specific humidity *sh* and atmospheric temperature *T* most closest to the cloud observations in both space and time are extracted and further interpolated in the vertical direction to match the bin numbers and sizes of the cloud mask profile. Then, we follow the method used by Di Giuseppe and Tompkins (2015) to project the *u* and *v* winds of every vertical bin onto the satellite overpass track, averaging in the along-track direction for all profiles in the selected CloudSat data segment (see section 2.3) to derive the scene-average, along-track horizontal wind *V* and the corresponding wind shear. Here, we define the wind shear $dV/dz_{i,j}$ between the layers *i* and *j*, which is used to calculate the cloud overlap parameter as follows:

$$dV/dz_{i,j} = \frac{\max\{V_i;V_j\} - \min\{V_i;V_j\}}{D_{i,j}}, \quad (1)$$

where V_i and V_j are the horizontal winds at layers *i* and *j*, respectively, and $D_{i,j}$ is the layer separation distance. For the CloudSat overpass track (Fig. 1a), Di Giuseppe and Tompkins (2015) indicated that the cross-track shear of the zonal wind *u* has little statistical significance.

Similarly with the wind shear, we calculate the vertical gradient of the saturation of the equivalent potential temperature ($\partial\theta_{es}/\partial z_{i,j}$) between the same two layers to quantify the dependence of the cloud overlap on the degree of the conditional instability of the moist convection. Here,

$$\theta_{es} = \theta \exp(\frac{L_v r_s}{C_p T})$$

$$\theta = T(\frac{1000}{p})^{0.286}, L_v = 2.5\times10^6 - 2323\times(T-273.16) \quad (2)$$

$$r_{s=} \frac{sh}{rh\times(1-sh)}$$

where θ is the potential temperature, L_v is the latent heat of vaporization, r_s is the saturation mixing ratio, C_p is the specific heat capacity at a constant pressure, and T is the atmospheric temperature. The smaller the $\partial\theta_{es}/\partial z_{i,j}$, the more unstable the atmosphere. Additionally, the scene-averaged vertical velocity at 500 hPa is extracted from the ERA-Interim reanalysis to analyze the impact of vertical motion on cloud overlap. In addition, to avoid artifacts due to noise from scattering of sunlight and minimize the uncertainty of the statistical results from the surface contamination of the CPR, only the nighttime datasets of cloud mask and meteorological parameters from 1 km above the TP surface are used to perform following analysis.

2.3 Retrieval of the overlap parameter and dependence on the spatial scale

Previous studies already have shown that the cloud overlap parameter is sensitive to the spatial scale of the GCM's grid box (Hogan and Illingworth, 2000; Oreopoulos and Khairoutdinov, 2003; Oreopoulos and Norris, 2011). For example, Hogan and Illingworth (2000) found that cloud overlap parameter tends to increase with decreasing spatial and temporal resolution (that is, with an increasing vertical and horizontal scale of GCMs). Thus, to discuss the dependence of overlap parameter over TP on the spatial scale, each CloudSat orbit over the TP region is divided into different segments based on the horizontal length of the segment (e.g., 25, 50, 100 and 200 km; for convenience, this length is referred to as the spatial scale of the GCM's grid box).

Fig 1b shows a sample cloud mask over the TP region derived from the 2B-GEOPROF-lidar dataset. This cloud mask includes eight, four, two and one segments

with lengths of 25, 50, 100 and 200 km, respectively. For each segment, the segment-average cloud cover profile is derived first. Then the vertical overlap between any two atmospheric layers in this profile is calculated when the cloud covers (C_i and C_j) of both layers exceed 0. Following the examples of previous studies (Hogan and Illingworth, 2000; Di Giuseppe and Tompkins, 2015), we consider nonadjacent layers to be a continuous cloud pair when all layers between them are classified as cloudy. Otherwise, these layers are classified as a discontinuous cloud pair (Hogan and Illingworth, 2000; Di Giuseppe and Tompkins, 2015). By using random, maximum and minimum assumptions of overlap, the total cloud covers of any two cloud layers are given by

$$\begin{aligned} C_{i,j}^{ran} &= C_i + C_j - C_i \times C_j, \\ C_{i,j}^{\max} &= \max\{C_i, C_j\}, \\ C_{i,j}^{\min} &= \min\{1, C_i + C_j\}, \end{aligned} \tag{3}$$

Further, we use the definition of Hogan and Illingworth (2000) to quantify the degree of cloud overlap using the "overlap parameter" α, which is calculated using the following formula:

$$C_{i,j}^{obs} = \alpha C_{i,j}^{\max} + (1-\alpha) C_{i,j}^{ran} \tag{4}$$

The overlap parameter α can thus be written as follows:

$$\alpha = \frac{C_{i,j}^{obs} - C_{i,j}^{ran}}{C_{i,j}^{\max} - C_{i,j}^{ran}} \tag{5}$$

Eq. 4 indicates that the parameter α ranges from 0 (random) to 1 (maximum) when the total observed cloud cover falls between the values derived using the maximum and random overlap assumptions. However, α may be negative when the degree of cloud overlap is lower than that predicted by the random overlap assumption.

Fig.2a and 2b test the sensitivity of α to the spatial scale for both discontinuous and continuous cloud pairs. Many previous studies have used ground- and space-based radar to verify the validity of the random overlap assumption for the vertically discontinuous clouds (Hogan and Illingworth, 2000; Mace at al., 2002; Naud et al., 2008; Di Giuseppe and Tompkins, 2015). Our results show that the degree of cloud overlap of the discontinuous clouds over the TP region is lower than that of random overlap, especially

when layer distance is smaller. Given the spatial scale (e.g., 50 km), almost all the α values are negative and fall between -0.25 and -0.05. Thus, the total cloud cover is still slightly underestimated for discontinuous cloud pairs when using the random overlap assumption. Assuming a cloud layer distance of less than 9 km, α for discontinuous cloud pairs increases as the spatial scale increases (e.g., from 25 km to 200 km). For a continuous cloud pair, we found that the value of α decreased gradually from 0.95 to 0 with increasing distance. Meantime, the dependence of α on the spatial scale is also observed for continuous cloud pairs when they are separated by a distance of less than 9 km (Fig. 2b), especially when layer distance is smaller than 5km. This correlation indicates that a maximum overlap is more common for a larger domain, which is consistent with the results of previous studies (Hogan and Illingworth, 2000; Oreopoulos and Khairoutdinov, 2003; Oreopoulos and Norris, 2011).

2.4 Selection of thresholds for cloud cover and spatial scale

About the dependence of α on the spatial scale, Tompkins and Di Giuseppe (2015) provided some heuristic discussions and attributed the phenomena to a data truncation error. Simply, these authors theorized that some overcast or single cloud layers will be removed from the samples when the spatial scale is smaller than the cloud system scale, thus biasing α and its decorrelation length. Given a spatial scale of 50 km, the ratio of the spatial scale to the cloud system scale decreases strongly from the equator to the poles because many of the frontal cloud systems of the middle and high latitudes are larger than the convective cloud systems over the tropics. Ultimately, the corresponding bias of α will increase with latitude. Thus, regional atmospheric models should account for the typical cloud system scales when they are applied at a fixed horizontal resolution.

Fig. 2c depicts the probability distribution functions (PDFs) of the horizontal scales of the along-track cloud systems at different heights over the TP region. Here, the horizontal scale of a cloud system at a given height along the CALIPSO/CloudSat track is determined by calculating the number of continuous cloud profiles (N) at a given height. Using a 1.1 km along-track resolution for the CPR measurements, the along-track scale (S in km) of a cloud system is $S=N\times1.1$ (Zhang et al., 2014; Li et al., 2015). It is clear that the probability of a small-scale cloud system decreases with increasing height. On average, the horizontal scale of a cloud system at a height of 15 km (mean value: 59.2 km)

is almost twelve times greater than that at a height of 2 km (mean value: 4.6 km). From the statistical results shown in Fig. 2c, we apply a spatial scale of 50 km to perform following analysis although this scale will still result in large retrieval errors of α at higher atmospheric heights (e.g., 15km) where cloud has large horizontal scale.

To further reduce the inversion errors of α and its sensitivity to the spatial scale caused by data truncation, we follow the suggestion of Tompkins and Di Giuseppe (2015) and apply a simple data filter so that only atmospheric layers with segment-average cloud covers smaller than a given threshold of 50% are retained. As stated by Tompkins and Di Giuseppe (2015), data will still be truncated with this filter, but the sensitivity of the results to the spatial scale should be reduced. Although limiting the spatial scale (50 km) and upper limit of cloud cover (50%), the number of available samples is still at least one million, thus ensuring statistical significance. Fig. 2d shows the number of samples and the percentages at different cloud layer distances for both discontinuous and continuous clouds. These results clearly show that the proportion of cloud samples with smaller layer distances (e.g., 4 km) accounts for 90% of all samples of continuous clouds. Here, it is important to reiterate that cloud fraction and cloud cover are different variables in our study. The "*Cloud fraction*" reports the fraction of lidar volumes in each radar vertical bin that contains hydrometeors and is used to identify a cloudy atmospheric bin based on the chosen threshold, which is 99% in this paper. When averaging in the along-track direction for all cloud fraction profiles in a selected CloudSat data segment, we derive the segment-average cloud covers profile, which represents the percentage of clouds in a given spatial scale and certain height. Given the 1.1 km along-track resolution of the CPR measurements and a spatial scale of 50 km, the segment-averaged cloud cover implies that the cloud cover is resolvable to approximately 2% (Di Giuseppe and Tompkins, 2015).

3. Results

3.1 Monthly and zonal variations of the overlap parameter for continuous clouds

Figure 3a shows the monthly variations for the continuous cloud-pair related pentad-averaged α over the TP. In Fig.3a, the maximum continuous cloud layer distance over the TP gradually increases from January (approximately 6 km) to August (beyond 8 km) and then gradually decreases. It means that cloud systems over TP during summer

are thicker than other seasons. When the cloud layer distance is less than 1.5 km, we find that the overlap parameter α has little monthly variation and always large (even beyond 0.7). However, the monthly variation of α becomes manifest with increasing layer distance. For example, given a 2-km cloud distance, α reaches its maximum and minimum values in August (0.45) and February (0.1) (see Fig. 3d). As this distance increases (e.g., to 3 km), α is generally lower but has the similar monthly variations to those seen at the 2-km distance. It is clear that even random overlap assumption will also underestimate the total cloud cover between two cloud layers with large distance during all seasons except summer. Actually, these cloud overlap features may be associated with the unique topographical forcing and thermo-dynamical environment of the TP. In summer, the TP is usually considered to be an atmospheric heat source or "air pump" due to its higher surface temperature compared with surrounding regions at the same altitude (Wu et al., 2015). Additionally, a humid and warm air intrudes from the South Asia monsoon area into the lower atmosphere over the TP to intensify the atmospheric instability of moist convection when combined with the enhanced surface heating (Taniguchi and Koike, 2008). This process further promotes the transportation of water vapor into high altitudes and favors the development of convective clouds. Indeed, satellite observations have indicated that cumulus prevails over the TP during the summer (Wang et al., 2014; Li and Zhang, 2016).

Because of the small horizontal scale of cumulus, 50 km-sampling scale from CloudSat should not bias α too much in our study. However, previous studies have pointed out that precipitation may bias the cloud overlap statistics toward maximum overlap (Mace et al., 2009; Di Giuseppe and Tompkins). Present study doesn't eliminate the influence of precipitation on the overlap parameter, which means that overlap parameter α will be smaller if cloud samples with precipitation are removed from our analysis. The feature may be even more obvious during summer due to more frequent precipitation over TP occurs this season (Yan et al., 2016). The seasonal variation of α was also found at different ground sites (Mace and Benson-Troth, 2002; Naud et al., 2008). For example, Oreopoulos and Norris (2011) indicated that clouds tend to be more random in the winter and most maximum during the summer. In fact, these overlap properties are associated with cloud system scale, which is dominated by dynamical

situation (Tompkins and Di Giuseppe, 2015).

In the Fig. 3b and 3c, we also present the monthly variations for the continuous cloud-pair related pentad-averaged the degree of conditional instability of the moisture convection $\partial\theta_{es}/\partial z$ and the wind shear dV/dz over the TP, respectively. Same as the α, the corresponding $\partial\theta_{es}/\partial z$ and dV/dz both exhibit obvious monthly variations as well. The atmospheric stability and wind shear gradually decrease from January to August and then steadily increase (see Figs. 3b, 3c, 3e and 3f). From the Fig.3b, we can see that adjacent atmospheric layers during May and September tend to be more instability and have weak wind shear. These atmospheric states favor the development of clouds and result in maximum overlap between cloud layers. During other month (e.g., December), clouds also tend to be more maximum although adjacent atmospheric layers is stable (e.g. large $\partial\theta_{es}/\partial z$ and dV/dz). As the increasing of layer distance, atmospheric layers become stable and favor random overlap, especially during summer season. These results verify that a more unstable atmosphere tends to favor a maximum overlap over a random one, which is consistent with previous studies (Mace and Benson-Troth, 2002; Naud et al., 2008). In addition, Figs. 3e and 3f also reveal an inconsistency in the relationship of layer distance and the corresponding wind shear and atmospheric stability. For example, we can see that the wind shear for a 2-km layer distance is greater than that for a 3-km distance, but the atmosphere is also more unstable. This difference is probably because two cloud layers with the same separation but different altitudes are sorted into the same statistical group.

Additionally, Fig. 4 shows the zonal variations of α, $\partial\theta_{es}/\partial z$ and dV/dz over the TP. Figs. 4a and 4d clearly indicate that α is larger to the south part of the TP and smaller to the north. This is mainly due to instability atmosphere over the southern part of the TP enhances the convective activity than over the northern part (Fujinami and Yasunari, 2001). Due to the weakening of the monsoon and the blocking by topography, less water vapor may reach the northern part, thus cause fewer clouds over this part (You et al., 2014). However, compared with southern part of the TP, the stability and wind shear are both larger over the northern part, especially for those cloud layer with large distance. This dynamical condition will result in more frequent negative α and thus

means that random overlap assumption used in models will underestimate the total cloud cover and bias the surface radiation over these regions (see Fig.4a). At present, some studies have contributed the most significant warming occurring over the Northern part of TP to pronounced stratospheric ozone depletion (e.g., Guo and Wang, 2012). However, a recent study indicates that accelerated warming trend over the Tibetan Plateau may be due to the rapid cloud cover increases at nighttime over the northern Tibetan Plateau and the sunshine duration increase in the daytime over the southern Tibetan Plateau (Duan and Xiao, 2015). It means that the reasonable representation of total cloud cover in model is very important to the understanding of the TP rapid warming. Although models are still difficult to capture the cloud overlap properties, especially for those cloud layer with large distance over north TP, our statistical results confirm that α is very well correlated with wind shear and instability.

Besides the wind shear and instability, some studies also tested the sensitivity of the overlap parameter to the large-scale vertical velocity. For example, Naud et al. (2008) found a weak sensitivity of α to vertical velocity, and attributed it to the uncertainty in the reanalysis dataset. For comparison, we also analyze the monthly and zonal variations of the 500 hPa vertical velocity over the TP (see the Figs. s1 and s2 in the supplementary material). Although the monthly cycle of α is related to the local vertical velocity, the zonal variation of α is inconsistent with the variation of vertical velocity. In addition, we also find that the sensitivity of α is relative weaker than other parameters (see the Fig.s3). As a result, a parameterization of α with consideration of the impact of wind shear and instability should improve the simulation of total cloud cover in the climate models.

3.2 The sensitivity of overlap parameter to dynamical factors and parameterization

To facilitate the parameterization of α for cases of continuous clouds, we further investigate the sensitivity of α to different meteorological conditions. Here, each meteorological factor over the TP region is grouped into one of four bins based on its values. In the present study, the four bins for $\partial\theta_{es}/\partial z$ are $\partial\theta_{es}/\partial z > 5$ K/km, $2.5 < \partial\theta_{es}/\partial z < 5$ K/km, $0 < \partial\theta_{es}/\partial z < 2.5$ K/km and $\partial\theta_{es}/\partial z < 0$ K/km. For wind shear, the four bins are $dV/dz < 0.5$ m • s^{-1}/km, $0.5 < dV/dz < 2$ m • s^{-1}/km, $2 < dV/dz < 3.5$

m • s^{-1}/km and $dV/dz > 3.5$ m • s^{-1}/km. These groupings ensure that a statistically significant number of samples fall within each bin (i.e., at least one hundred thousand samples per bin).

Fig. 5 illustrates the sensitivity of α to wind shear and instability at given upper limit of cloud cover (50%) for the continuous clouds. When considering the proportion of cloud samples with small layer distances (<3.5 km), which account for 90% of all samples with continuous clouds, we only provide the statistical results for layer distances smaller than 3.5 km. In the Fig.5, it is clear that the dependence of α on dV/dz seems relative weaker compared with $\partial\theta_{es}/\partial z$. The dependence is more obvious when the layer distance is larger than 1.5 km. Naud et al. (2008) tested the sensitivity of α to wind shear at three sites and found that wind shear slightly affects α when the layer distance is larger than 2 km. However, in a recent study, Di Giuseppe and Tompkins (2015) demonstrated the important effect of wind shear on the global cloud overlap by using a combination of the CloudSat-CALIPSO cloud data and the ECMWF reanalysis dataset. These results and our own results demonstrate that variations in cloud overlap are closely related to atmospheric dynamics, but their relationship is not stable and has spatial variations. Shortly, the effect of the atmospheric stability in cloud overlap may be more important over convective regions (e.g., the intertropical convergence zone and TP during summer season), while the effect of wind shear may be dominant over the mid-latitudes.

As we know, the overlap parameter α for continuous cloud layers can be modeled as an inverse exponential function:

$$\alpha = e^{-D/L} \tag{6}$$

where *D* is the layer separation distance and *L* is the decorrelation length scale that characterizes the transition from the maximum to random overlap assumption. In previous studies, it is found that *L* depends on the vertical and temporal resolutions of the lidar data or the spatial scale of the models, and the values of *L* have varied across many studies (Hogan and Illingworth, 2000; Mace and Benson-Troth, 2002; Pincus et al., 2005). For example, Barker (2008) found a wide range of *L* values, with a median value of 2 km, when analyzing the global CloudSat and CALIPSO datasets. Oreopoulos and Norris (2011) derived *L* based on radar measurement taken over the Southern Great Plains (SGP)

of the USA. Their results indicated that the value of L ranges from 2 to 4.5 km across different seasons and that smaller spatial scales correspond with smaller L values. In other studies, L was usually a function of latitude or total cloud cover (Shonk et al., 2010; 2014; Yoo et al., 2014).

In the following study, we derive the L values (unit: km) from the least squares exponential fit to the original α curve at given wind shear and instability bin. Then, further parameterize L as a function of wind shear or atmospheric instability based on both a multiple linear regression method and our statistical dataset. The regression formula of L can be written as:

$$L = L_{\alpha} - b1\frac{\partial \theta_{es}}{dz} - b2\frac{dV}{dz}$$
$$or \qquad (7)$$
$$L = L_{\alpha 1} - c1\frac{dV}{dz}$$

Here, L_{α} , $L_{\alpha 1}$, $b1$,$b2$,and $c1$ are the fitting parameters. Table 1 lists several parameterization schemes for the decorrelation length scale L. The Di Giuseppe/Wind scheme is the previously mentioned scheme from Di Giuseppe and Tompkins (2015), i.e., using the global CloudSat-CALIPSO cloud data and ECMWF reanalysis dataset to parameterize L as a function of wind shear. In their study, Di Giuseppe and Tompkins showed some uncertainties from fitting methods and calculation of wind shear. Indeed, due to the radiosonde data with high temporal and spatial resolutions is very scarce over the TP, it is hard to derive accurate wind shear collocated with cloud profile from CloudSat observations, especially for cloud layers with smaller layer separations. In addition, due to the observation orbit, the impact of cross-track wind shear is still neglected in our study, which would exclude many large wind shear related with jet structures, especially in the tropics and mid-latitudes (Di Giuseppe and Tompkins, 2015). The method of Shonk et al. (2010) is also used, which proposed an empirical linear relationship between L and latitude (see Shonk/Latitude scheme) by using CloudSat and CALIPSO data. The Li/wind and Li/Wind-Instability schemes are derived from this study based on Equ.(7). For detailed information about each scheme, see the descriptions in Table 1. Note that the R-squared values (R^2) for Li/wind and Li/Wind-Instability schemes are 0.88 and 0.96, respectively.

Fig. 6 presents the monthly difference between calculated and observed cloud covers for the aforementioned schemes and indicates that the maximum and random overlap assumptions result in large cloud cover biases at most of the layer distances, especially for layer distances greater than 1 km and less than 2 km (where the bias exceeds 5%). Compared with random and maximum assumptions, other schemes have the small cloud cover bias. However, several points still require further interpretation. First, Di Giuseppe/Wind scheme still obviously underestimates the cloud cover for layer distances above 1 km (e.g., reach 3%). Notably, the large bias of this scheme may occur because it is based on the global CloudSat-CALIPSO measurements and ECMWF reanalysis dataset for a short period (January-July 2008); as such, some obvious regional or seasonal cloud overlap properties are easily obscured by global averaging. Another possible cause is that the other dynamic factors (e.g., the atmospheric stability) were not considered in the parameterization of this scheme. However, Giuseppe/Wind scheme also cause little bias for layer distances below 1 km, because it retrieves much larger L and overlap parameter values than other schemes. Second, an interesting finding is that Shonk/Latitude scheme leads to comparable bias with new schemes from this study. Even, the bias is much smaller for Shonk/Latitude scheme when layer distances below 1 km. In fact, the Fig.5 has demonstrated that the sensitivity of α to wind shear and instability is rather weak when cloud layers are very close. It further shows that new schemes are still difficult to capture the cloud overlap properties between close cloud layers due to the rare of radiosonde data over the TP. Third, latter four schemes all produce small bias during summer, whereas underestimations are obvious during other seasons. Compared with Li/Wind scheme, Li/Wind-Instability scheme further combines the impact of atmospheric instability and has a relatively lower bias at large layer distances but higher R-squared values (R^2=0.96).

Fig.7 shows the zonal difference between calculated and observed cloud covers for the aforementioned schemes. The biases caused different schemes are distinguishable. For close cloud layers, Li/Wind and Li/Wind-Instability schemes are still cause slightly overestimation. For two cloud layer with large distances (e.g., 1 km), Giuseppe/Wind and Shonk/Latitude schemes results in a underestimation of total cloud cover, especially for Giuseppe/Wind scheme (reach 3%). In summary, this new scheme improves the

prediction of cloud cover over TP when cloud layers distances are above 1km.These results indicate that the effects of both wind shear and atmospheric stability on cloud overlap should be accounted for in the parameterization of the overlap parameter α over the TP.

4. Conclusions and discussion

The Tibetan Plateau has experienced obvious climate changes over the past three decades, and these climate changes (e.g., glacier retreat and permafrost degradation) are closely related with rapid warming over TP. Some studies have contributed the most significant warming occurring over the Northern part of TP to pronounced stratospheric ozone depletion (e.g., Guo and Wang, 2012). However, other study suggests that cloud cover exhibits a strong negative correlation with the diurnal temperature range and may explain different trends in the daytime and nighttime temperatures warming over the TP (Duan and Wu, 2006; Kang et al., 2010). Indeed, many studies have verified that annual and seasonal total cloud amounts have declined over TP (e.g., Yang et al., 2012; You et al., 2014), which induce the daytime sunshine duration to increase and result in surface air temperature warming (Duan and Xiao, 2015).

To accurately predict the total cloud cover and related to the radiative budget calculations, climate models need to reasonably represent the cloud vertical overlap, which has received less attention than necessary because of the limited regional cloud observations. In this study, we collect 4 years (2007–2010) of data from the CloudSat 2B-GEOPROF-LIDAR dataset, the ECMWF-AUX dataset and ERA-Interim daily 6-hourly reanalysis to verify that continuous cloud layers tend to maximum overlap at small distance but gradually randomly overlapped with increasing of layer distance. Focusing on the continuous cloud layers, we evaluate the effects of atmospheric dynamics on cloud overlap and find that the unstable atmospheric stratification and correspondingly weak wind shear over the TP lead to greater α values, which is well agreement with the results reported in previous studies. Finally, by using multiple linear regression method, we parameterize decorrelation length scale *L* as a function of the wind shear and atmospheric stability. Compared with other parameterizations, this new scheme slightly improves the prediction of cloud cover over TP when cloud layers distances are above 1km. Although the parameterization method derived in our study focuses on only

the TP and may therefore have some limitations for global applications, our results suggest that the parameterization of the decorrelation length scale *L* through the related physical processes and the consideration of multiple dynamic factors and microphysical effects (e.g., precipitation) has the potential to improve simulations of the total cloud cover in models.

In a recent study, Di Giuseppe and Tompkins (2015) applied the wind shear-dependent decorrelation length scale in the ECMWF Integrated Forecasting System, and found that the impact of wind shear-dependent parameterization on radiative budget calculation is comparable in magnitude to that of latitude-dependent scheme of Shonk et al. (2010). Our statistical results also show that latitude-dependent scheme has similar bias of cloud cover relative to new scheme. Although these results can't suggest which of the scheme is superior, the scheme based on dynamical factor has some potential advantages. For example, cloud overlap parameter is significantly controlled by atmospheric dynamics, therefore the long-term variations of meteorological factors are bound to affect the trend of cloud overlap and the following total cloud cover and radiation budget. Indeed, a recent study has shown that rapid warming and an increase of atmospheric instability over the TP leads to more frequent deep clouds, which are responsible to the reduction of solar radiation over the TP (Yang et al., 2012). In view of the decreasing trend of total cloud cover over this region (You et al., 2014), we may infer that the degree of cloud overlap over the TP possibly has an increasing trend. However, as stated by the Tompkins and Di Giuseppe (2015), true cloud overlap parameter will be biased at a given spatial sampling scale if one doesn’t consider the cloud system size. Thus whether the trend is true or significant over different parts of TP still needs further quantified because related cloud system scales over these regions are possibly changed as well.

Competing interests. The authors declare that they have no conflict of interest.

Acknowledgements. This research was jointly supported by the Foundation for Innovative Research Groups of the National Science Foundation of China (grant no. 41521004) and key Program of the National Natural Science Foundation of China

(41430425), National Science Foundation of China (grant nos. 41575015 and 41575143) and the China 111 project (grant no. B13045). We would like to thank the CALIPSO, CloudSat and ERA-Interim science teams for providing excellent and accessible data products that made this study possible.

References

Barker, H. W., Stephens, G. L., and Fu, Q.: The sensitivity of domain-averaged solar fluxes to assumptions about cloud geometry, Quart. J. R. Meteorol. Soc., 125, 2127-2152, 1999.

Barker, H. W.: Overlap of fractional cloud for radiation calculations in GCMs: A global analysis using CloudSat and CALIPSO data, J. Geophys. Res., 113(113), 762-770, 2008.

Boucher, O., Randall, D., Artaxo, P., Bretherton, C., Feingold, G., Forster, P., Kerminen, V.-M., Kondo, Y., Liao, H., Lohmann, U., Rasch, P., Satheesh, S. K., Sherwood, S., Stevens, B., and Zhang, X. Y.: Clouds and aerosols, in: Climate Change 2013: The Physical Science Basis. Contribution of Working Group I to the Fifth Assessment Report of the Intergovernmental Panel on Climate Change, edited by: Stocker, T. F., Qin, D., Plattner, G.-K., Tignor, M., Allen, S. K., Doschung, J., Nauels, A., Xia, Y., Bex, V., and Midgley, P. M.: Cambridge University Press, United Kingdom and New York USA, 571–657, doi:10.1017/CBO9781107415324.016, 2013.

Chang, F. L., and Li, Z.: A New Method for Detection of Cirrus Overlapping Water Clouds and Determination of Their Optical Properties, J. Atmos. Sci., 62(11), 3993-4009, 2005a.

Chang, F. L., and Li, Z.: A near global climatology of single-layer and overlapped clouds and their optical properties retrieved from TERRA/MODIS data using a new algorithm, J. Clim., 18, 4752–4771, 2005b.

Chen, B., and Liu, X.: Seasonal migration of cirrus clouds over the Asian Monsoon regions and the Tibetan Plateau measured from MODIS/Terra, Geophys. Res. Lett., 32(320), 67-106, 2005.

Chen, T., Rossow, W. B., and Zhang, Y.: Radiative Effects of Cloud-Type Variations, J. Clim., 13, 264-286, 2000.

Cheng, G. and Wu, T.: Responses of permafrost to climate change and their environmental significance, Qinghai – Tibet Plateau, J. Geophys. Res., 112 (F2), F02S03, 2007.

Dee, D. P., Uppala, S. M., Simmons, A. J., Berrisford, P., Poli, P., Kobayashi, S., Andrae, U., Balmaseda, M., A. Balsamo, G., Bauer, P., Bechtold, P., Beljaars, A. C. M., Van De Berg, L., Bidlot, J., Bormann, N., Delsol, C., Dragani, R., Fuentes, M., Geer, A., J. Haimberger, L., Healy, S. B., Hersbach, H., Hólm, E. V., Isaksen, L., Kållberg, P., Köhler, M., Matricardi, M., McNally, A. P., Monge-Sanz, B. M., Morcrette,J. J., Park, B. K., Peubey, C., De Rosnay, P., Tavolato, C., Thépaut, J. N., and Vitart, F.: The ERA-Interim reanalysis: configuration and performance of the data assimilation system, Quart. J. R. Meteorol. Soc., 137(656), 553-597, 2011.

Di Giuseppe, F., and Tompkins, A. M.: Generalizing Cloud Overlap Treatment to Include the Effect of Wind Shear, J. Atmos. Sci., 72, 2865-2876, 2015.

Duan, A., and Xiao, Z.: Does the climate warming hiatus exist over the Tibetan Plateau?, Scientific

Reports, 5, 13711, 2015.

Duan, A., Wang, M., Lei, Y. and Cui, Y.: Trends in summer rainfall over China associated with the Tibetan Plateau sensible heat source during 1980 – 2008, J. Clim., 26, 261 – 275, 2013.

Duan, A., and Wu, G.: Change of cloud amount and the climate warming on the Tibetan Plateau, Geophys. Res. Lett., 33(22), 395-403, 2006.

Duan, A. M., and Wu, G. X.: Role of the Tibetan Plateau thermal forcing in the summer climate patterns over subtropical Asia, Clim. Dyn., 24(7), 793-807, 2005.

Fu, Q.,. Cribb, M.C Barker, H.W. Krueger, S.K. and Grossman, A. 2000: Cloud geometry effects on atmospheric solar absorption, J. Atmos. Sci., 57, 1156-1168, 2000;

Fujinami, H., and Yasunari, T.: The seasonal and intraseasonal variability of diurnal cloud activity over the Tibetan Plateau, J. Meteor. Soc. Japan, 79, 1207–1227, 2001.

Guo, D., and Wang, H.: The significant climate warming in the northern Tibetan Plateau and its possible causes, Int. J. Climatol. 32, 1775 – 1781. http://dx.doi.org/10.1002/joc.2388, 2012.

Haladay, T., and Stephens, G.: Characteristics of tropical thin cirrus clouds deduced from joint CloudSat and CALIPSO observations, J. Geophys. Res., 114(114), D00A25-D00A37, 2009.

Hartmann, D. L., Ockert-Bell, M. E., and Michelsen, M. L.: The effect of cloud type on Earth's energy balance: Global analysis, J. Clim., 5(11), 1281-1304, 1992.

Hogan, R. J., and Illingworth, A. J.: Deriving cloud overlap statistics from radar, Quart. J. R. Meteorol. Soc., 126(569), 2903-2909, 2000.

Huang, J. P., Minnis, P., and Lin, B.: Determination of ice water path in ice- over-water cloud systems using combined MODIS and AMSR-E measurements, Geophys. Res. Lett., 33, L21801, doi: 10.1029/2006GL027038, 2006a.

Huang, J. P.: Analysis of ice water path retrieval errors over tropical ocean, Adv. Atmos. Sci., 23, 165–180, 2006b.

Huang, J. P., Minnis, P., and Lin, B.: Advanced retrievals of multilayered cloud properties using multispectral measurements, J. Geophys. Res., 110, D15S18, doi: 10.1029/2004JD005101, 2005.

Jing, X., Zhang, H., Peng, J., Li, J., and Barker, H. W.: Cloud overlapping parameter obtained from CloudSat/CALIPSO dataset and its application in AGCM with McICA scheme, Atmos. Res., 170, 52-65, 2016.

Jing, X., Zhang H., and Guo P.: A study of the effect of sub-grid cloud structure on global radiation in climate models, Acta. Meteor. Sinica, 67, 1058-1068, 2009.

Kang, S., Xu, Y., You, Q., Flügel, W.A., Pepin, N. and Yao, T.: Review of climate and cryospheric change in the Tibetan Plateau, Environ. Res. Lett., 5, 015101. http://dx.doi.org/10.1088/1748-9326/5/1/015101, 2010.

Kato, S., Sun-Mack, S., Miller, W. F., Rose, F. G., Chen, Y., Minnis, P., and Wielicki, B. A.: Relationships among cloud occurrence frequency, overlap, and effective thickness derived from CALIPSO and CloudSat merged cloud vertical profiles, J. Geophys. Res., 115(D4), 1-28, 2010.

Kawamoto, K. and Suzuki, K.: Microphysical transition in water clouds Over the Amazon and China derived from spaceborne radar and Radiometer data, J. Geophys. Res., 117, D05212, doi: 10.1029/2011JD016412, 2012.

Li, J., Huang, J., Stamnes, K., Wang, T., Lv, Q., and Jin, H.: A global survey of cloud overlap based on CALIPSO and CloudSat measurements, Atmos. Chem. Phys., 15(1), 519-536, 2015.

Li, J., Hu, Y., Huang, J., Stamnes, K., Yi, Y., and Stamnes, S.: A new method for retrieval of the extinction coefficient of water clouds by using the tail of the CALIOP signal, Atmos. Chem. Phys., 11(6), 2903-2916, 2011.

Li, J., Yi, Y., Minnis, P., Huang, J., Yan, H., Ma, Y., Wang, W., and Ayers, K.: Radiative effect differences between multi-layered and single-layer clouds derived from CERES, CALIPSO, and CloudSat data, J. Quant. Spectrosc. Radiat. Transf., 112, 361-375, 2011.

Li, Y., Liu, X., and Chen B.: Cloud type climatology over the Tibetan Plateau: A comparison of ISCCP and MODIS/TERRA measurements with surface observations, Geophys. Res. Lett., 33, L17716, doi: 10.1029/2006GL026890, 2006.

Li, Y. Y., and Zhang, M.: Cumulus over the Tibetan Plateau in the summer based on CloudSat–CALIPSO data, J. Climate, 29, 1219–1230, doi:10.1175/JCLI-D-15-0492.1, 2016.

Mace, G. G., and Zhang, Q.: The CloudSat radar-lidar geometrical profile product (RL-GeoProf): Updates, improvements, and selected results, J. Geophys. Res., 119(15), 9441-9462, doi: 10.1002/2013JD021374, 2014.

Mace, G. G., Zhang, Q., Vaughan, M., Marchand, R., Stephens, G., Trepte, C., and Winker, D.: A description of hydrometeor layer occurrence statistics derived from the first year of merged CloudSat and CALIPSO data, J. Geophys. Res., 114, D00A26, doi: 10.1029/2007JD009755, 2009.

Mace, G. G., and Bensontroth, S.: Cloud-Layer Overlap Characteristics Derived from Long-Term Cloud Radar Data, J. Clim., 15(17), 2505-2515, 2002.

Morcrette, J. J., and Jakob, C.: The response of the ECMWF model to changes in the cloud overlap assumption, Mon. Wea. Rev., 128, 1707–1732, 2000.

Morcrette, J. J., and Fouquart, Y.: The Overlapping of Cloud Layers in Shortwave Radiation Parameterizations, J. Atmos. Sci., 43(4),321-328, 1986.

Naud, C. M., Del Genio, A., Mace, G. G., Benson, S., Clothiaux, E. E., and Kollias, P.: Impact of dynamics and atmospheric state on cloud vertical overlap, J. Clim., 21(8), 1758-1770, 2008.

Oreopoulos, L., and Norris, P. M.: An analysis of cloud overlap at a midlatitude atmospheric observation facility, Atmos. Chem. Phys., 11(1), 5557-5567, 2011.

Oreopoulos, L., and Khairoutdinov, M.: Overlap properties of clouds generated by a cloud-resolving model, J. Geophys. Res., 108, 4479, doi: 10.1029/2002JD003329, 2003.

Pincus, R., Hannay, C., Klein, S. A., Xu, K. M., and Hemler, R.: Overlap assumptions for assumed probability distribution function cloud schemes in large-scale models, J. Geophys. Res., 110(D15), 2005.

Rossow, W. B., Gardner, L. C., and Lacis, A. A.: Global seasonal cloud variations from satellite radiance measurements. Part I: sensitivity of analysis, J. Clim., 2, 419-458, 1989.

Shonk, J. K. P., Hogan, R. J., and Manners, J.: Impact of improved representation of horizontal and vertical cloud structure in a climate model, Clim. Dyn., 38, 2365-2376, 2014.

Shonk, J. K., Hogan, R. J., Edwards, J. M., and Mace, G. G.: Effect of improving representation of

horizontal and vertical cloud structure on the Earth's global radiation budget. Part I: Review and parametrization, Quart. J. R. Meteorol. Soc., 136(650), 1191-1204, 2010.

Stephens, G. L.: Cloud feedbacks in the climate system: a critical review, J. Clim., 18, 237-273, 2005.

Stephens, G. L., Vane, D. G., Boain, R. J., Mace, G. G., Sassen, K., Wang, Z., Illingworth, A. J., O'Connor, E. J., Rossow, W. B., Durden, S. L., Miller, S. D., Austin, R. T., Benedetti, A., Mitrescu, C., and CloudSat Science Team.: The CloudSat mission and the A-Train, A new dimension of space-based observations of clouds and precipitation, B. Am. Meteor. Soc., 83, 1771-1790, 2002.

Taniguchi, K., and Koike, T.: Seasonal variation of cloud activity and atmospheric profiles over the eastern part of the Tibetan Plateau. J. Geophys. Res., 113(D10), 523-531, 2008.

Tompkins, A., and Giuseppe, F. D.: An interpretation of cloud overlap statistics, J. Atmos. Sci., 72, 2877-2889, 2015.

Verlinden, K. L., Thompson, D. W. J., and Stephens, G. L.: The Three-Dimensional Distribution of Clouds over the Southern Hemisphere High Latitudes, J. Clim., 24(24), 5799-5811, 2011.

Willén, U., Crewell, S., Baltink, H. K., and Sievers, O.: Assessing model predicted vertical cloud structure and cloud overlap with radar and lidar ceilometer observations for the Baltex Bridge Campaign of CLIWA-NET, Atmos. Res., 75(3), 227-255, 2005.

Winker, D. M., Hunt, W. H. and McGill, M. J.: Initial performance assessment of CALIOP, Geophys. Res. Lett., 34(19), 228-262, 2007.

Wang, B., Bao, Q., Hoskins, B., Wu, G. and Liu, Y.: Tibetan Plateau warming and precipitation changes in East Asia, Geophys. Res. Lett., 35, L14702, 2008

Wang, M. Y., Gu, J., Yang, R., Zeng, L. and Wang, S.: Comparison of cloud type and frequency over China from surface, FY-2E, and CloudSat observations. Remote Sensing of the Atmosphere, Clouds, and Precipitation, E. Im, S. Yang, and P. Zhang, Eds., International Society for Optical Engineering (SPIE Proceedings, Vol. 9259), doi:10.1117/12.2069110, 2014.

Wang, W., Huang, J., Minnis, P., Hu, Y., Li, J., Huang, Z., Ayers, J. K., and Wang, T.: Dusty cloud properties and radiative forcing over dust source and downwind regions derived from A-Train data during the Pacific Dust Experiment, J. Geophys. Res., 115, D00H35, doi:10.1029/2010JD014109, 2010.

Wu, G., Duan, A., Liu, Y., Mao, J., Ren, R., Bao, Q., He, B., Liu, B., and Hu, W.: Tibetan Plateau climate dynamics: recent research progress and outlook, National Science Review, 2(1), 100-116, 2015.

Wu, G. X., Liu, Y., Wang, T., Wan, R., Liu, X., Li, W., Wang, Z., Zhang, Q., Duan, A., and Liang X.: The influence of the mechanical and thermal forcing of the Tibetan Plateau on the Asian climate, J. Hydrometeorol., 8, 770–789, doi:10.1175/JHM609.1, 2007.

Wu, H., Yang, K., Niu, X., and Chen, Y.: The role of cloud height and warming in the decadal weakening of atmospheric heat source over the Tibetan Plateau, Sci. China Ser. D., 58(3), 395–403, doi:10.1007/s11430-014-4973-6, 2015.

Xu, X., Lu, C., Shi, X., and Gao, S.: World water tower: An atmospheric perspective, Geophys. Res. Lett., 35(20), 525-530, 2008.

Yan, H.R., Li, Z.Q., Huang, J.P., Cribb, M., Liu, J.J.: Long-term aerosol-mediated changes in cloud radiative forcing of deep clouds at the top and bottom of the atmosphere over the Southern Great Plains，Atmos. Chem. Phys.,14(14), 7113-7124, 2014.

Yan, Y., Liu, Y. and Lu, J.: Cloud vertical structure, precipitation, and cloud radiative effects over Tibetan Plateau and its neighboring regions, J. Geophys. Res. Atmos., 121 (2016), pp. 5864-5877,10.1002/2015JD024591, 2016.

Yanai, M., Li, C. F., and Song, Z. S.: Seasonal heating of the Tibetan Plateau and its effects on the evolution of the Asian summer monsoon, J. Meteor. Soc. Japan, 70, 319–351, 1992.

Yang, K., Wu, H., Qin, J., Lin, C., Tang, W., and Chen, Y.: Recent climate changes over the Tibetan Plateau and their impacts on energy and water cycle: A review, Global and Planetary Change, 112(1), 79-91, 2014.

Yang, K., Ding B., Qin, J., Tang W., Lu, N., and Lin, C.,: Can aerosol loading explain the solar dimming over the Tibetan Plateau?, Geophys. Res. Lett., 39, L20710, doi: 10.1029/2012GL053733, 2012.

Yang, K., Guo, X., He, J., Qin, J. and Koike, T.: On the climatology and trend of the atmospheric heat source over the Tibetan Plateau: an experiments-supported revisit, J. Clim., 24, 1525–1541, 2011.

Yoo, H., Li, Z., You, Y., Lord, S., Weng F, and Barker H. W.: Diagnosis and testing of low-level cloud parameterizations for the NCEP/GFS model satellite and ground-based measurements, Clim. Dyn., 41(5-6), 1595-1613, doi:10.1007/s00382-013-1884-8, 2013.

You, Q., Jiao, Y., Lin, H., Min, J., Kang, S., Ren, G., and Meng, X.: Comparison of NCEP/NCAR and ERA-40 total cloud cover with surface observations over the Tibetan Plateau, International Journal of Climatology, 34(8), 2529-2537, 2014.

Yuan, T., and Oreopoulos, L.: On the global character of overlap between low and high clouds, Geophys. Res. Lett., 40, 5320-5326, 2013.

Zhang, H., and Jing, X.: Advances in studies of cloud overlap and its radiative transfer in climate models, J. Meteoro. Res., 30(2), 156-168, 2016.

Zhang, H., Peng, J., Jing, X., and Li, J.: The features of cloud overlapping in Eastern Asia and their effect on cloud radiative forcing, Science China Earth Sciences, 56(5), 737-747, 2013.

Zhang, H., and Jing, X. W.: Effect of cloud overlap assumptions in climate models on modeled earth-atmophere radiative fields, Chinese Journal of Atmospheric Sciences, 34(3), 520-532, 2010.

Zhao, C.F., Liu, L.P., Wang, Q.Q., Qiu, Y.M., Wang, Y., and Wu, X. L.: MMCR-based characteristic properties of non-precipitating cloud liquid droplets at Naqu site over Tibetan Plateau in July 2014, Atmospheric research, 190, 68-76, doi.org/10.1016/j.atmosres.2017.02.002, 2017.

Zhao, C.F., Liu, L.P., Wang, Q.Q., Qiu, Y.M., Wang, W., Wang, Y., and Fan, T.Y.: Toward Understanding the Properties of High Ice Clouds at the Naqu Site on the Tibetan Plateau Using Ground-Based Active Remote Sensing Measurements Obtained during a Short Period in July 2014, Journal of Applied Meteorology and Climatology, 55, 2493-2507,

doi:10.1175/JAMC-D-16-0038.1, 2016.

Zhu, L., Xie, M. and Wu, Y.: Quantitative analysis of lake area variations and the influence factors from 1971 to 2004 in the Nam Co basin of the Tibetan Plateau, Chin. Sci. Bull. 55, 1294 – 1303, 2010.

745

Table 1. Several parameterizations of decorrelation length scale L from the exponential fit as a function of atmospheric stability $\partial\theta_{es}/\partial z$, wind shear dV/dz or latitude Φ

Scheme	description	decorrelation length scale L
Random	Random	
Maximum	Maximum	
Di Giuseppe/Wind[1]	Random/Maximum, only wind shear	$L = 4.4 - 0.45 \times \frac{dV}{dz}$
Li/Wind[2]	Random/Maximum, only wind shear	$L = 2.19 - 0.14 \times \frac{dV}{dz}$
Li/Wind-Instability[3]	Random/Maximum, wind shear and instability	$L = 2.18 - 0.09 \times \frac{dV}{dz} - 0.15 \times \frac{\partial\theta_{es}}{dz}$
Shonk/Latitude[4]	Random/Maximum, only latitude	$L = 2.899 - 0.02759 \times \lvert \Phi \rvert$

750 [1]Scheme is based on Eq. (4), and decorrelation length scale L is parameterized as a function of wind shear (Di Giuseppe and Tompkins, 2015); [2]Scheme is based on Eq. (4), and decorrelation length scale L is parameterized as a function of wind shear based on our study; [3]Scheme is based on Eq. (4), and decorrelation length scale L is parameterized as a function of wind shear and instability based on our study; [4]Scheme is based on Eq. (4), and decorrelation length scale L is parameterized as a function of latitude (Shonk et al. , 2010).

755

760

765

770

775

Figure captions

780 Figure 1. (a) CloudSat overpass tracks (blue line: daytime; red line: nighttime) over the Tibetan Plateau (27 ℃N-39 ℃N; 78 ℃E-103 ℃E); (b) A sample of CloudSat 2B-GEOPROF-LIDAR cloud mask product along the ground track of 200km (white color: cloud fraction>99%; light blue: 0<cloud fraction<99%; deep blue: clear sky; orange color: surface).

785

Figure 2. (a), (b) The sensitivity of α to the spatial scale for non-continuous and continuous cloud pairs; (c) The probability distribution functions (PDFs) of the along-track horizontal scales of cloud system at different height over TP region; (d) Cloud sample numbers for the non-continuous and continuous clouds at a given sampling
790 scale of 50km. The percentages represent the proportions of cloud sample below corresponding layer distance to all samples.

Figure 3. (a),(b) and (c) The monthly variations of the pentad-averaged cloud overlap parameter α, degree of conditional instability to moist convection $\partial\theta_{es}/\partial z$ and wind
795 shear dV/dz for the continuous clouds over the TP ; (d), (e) and (f) The monthly variations of the pentad-averaged α, $\partial\theta_{es}/\partial z$ and dV/dz for the continuous clouds at given layer distances (red: 2km; black: 3km).

Figure 4. (a),(b) and (c) The zonal variations of the α, $\partial\theta_{es}/\partial z$ and wind shear dV/dz
800 for the continuous clouds over the TP; (d), (e) and (f) The zonal variations of the α, $\partial\theta_{es}/\partial z$ and dV/dz for the continuous clouds at given layer distances (red: 2km; black: 3km).

Figure 5. The variation of overlap parameter α with layer distance under different
805 large-scale dynamics. (a): wind shear and (b): instability.

Figure 6. The monthly difference of cloud cover between calculated and observed for

different schemes (see the Table 1) and its variation with layer distance.

Figure 7. The zonal difference of cloud cover between calculated and observed for different schemes (see the Table 1) and its variation with layer distance.

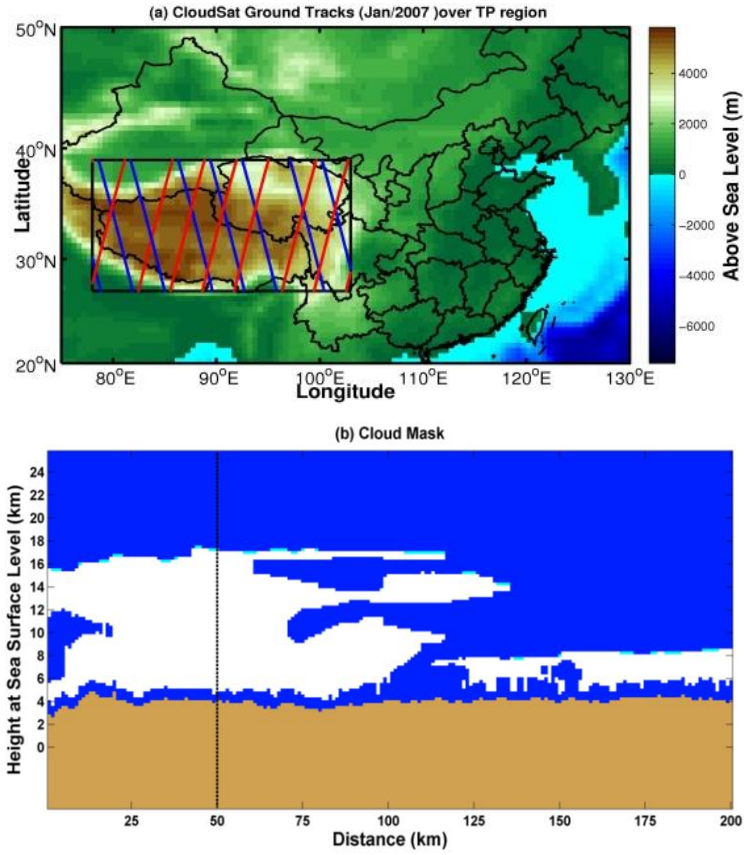

Figure 1. (a) CloudSat overpass tracks (blue line: daytime; red line: nighttime) over the Tibetan Plateau (27 ℕ-39 ℕ; 78 𝔼-103 𝔼); (b) A sample of CloudSat 2B-GEOPROF-LIDAR cloud mask product along the ground track of 200km (white color: cloud fraction>99%; light blue: 0<cloud fraction<99%; deep blue: clear sky; orange color: surface).

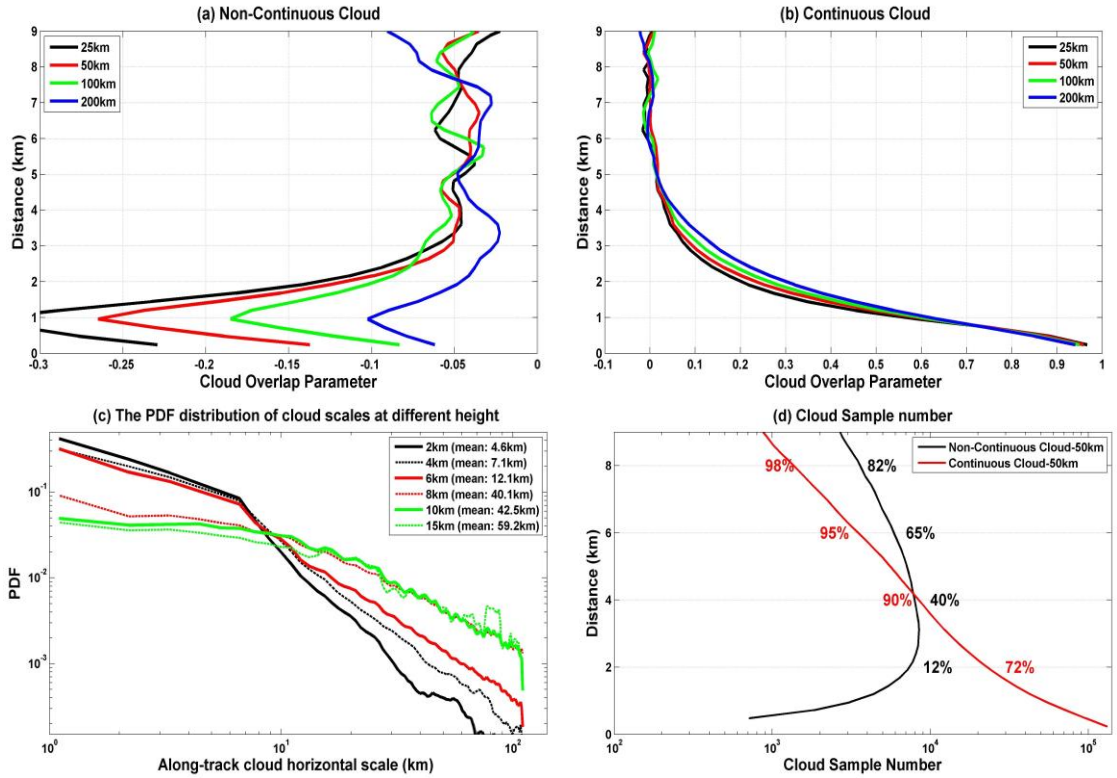

855 Figure 2. (a), (b) The sensitivity of α to the spatial scale for non-continuous and continuous cloud pairs; (c) The probability distribution functions (PDFs) of the along-track horizontal scales of cloud system at different height over TP region; (d) Cloud sample numbers for the non-continuous and continuous clouds at a given sampling scale of 50km. The percentages represent the proportions of cloud sample below
860 corresponding layer distance to all samples.

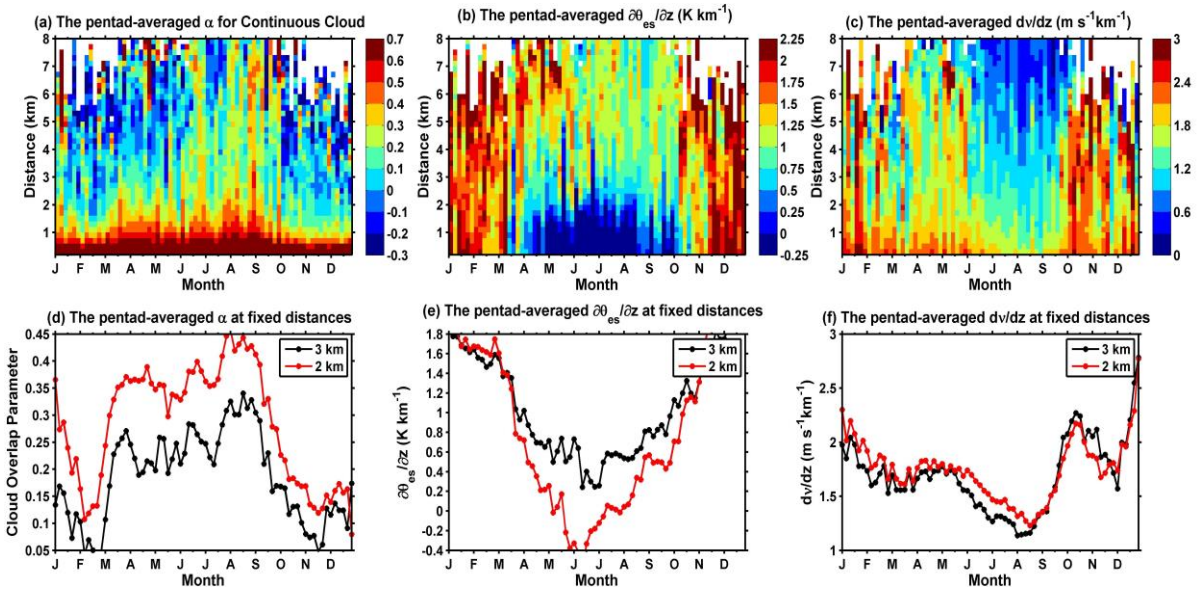

Figure 3. (a),(b) and (c) The monthly variations of the pentad-averaged cloud overlap parameter α, degree of conditional instability to moist convection $\partial\theta_{es}/\partial z$ and wind shear dV/dz for the continuous clouds over the TP ; (d), (e) and (f) The monthly variations of the pentad-averaged α, $\partial\theta_{es}/\partial z$ and dV/dz for the continuous clouds at given layer distances (red: 2km; black: 3km).

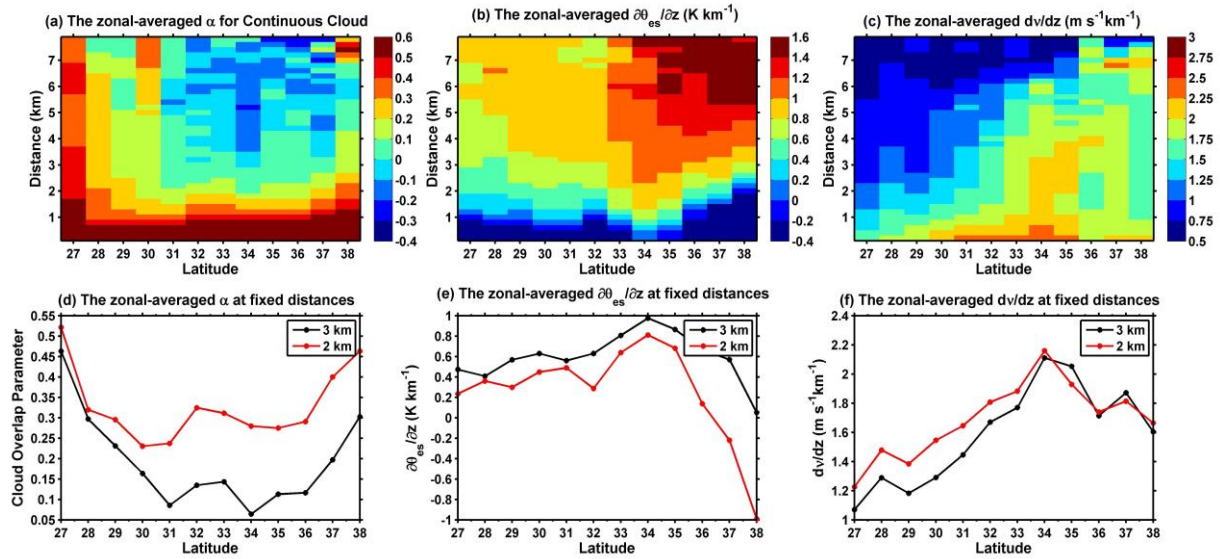

Figure 4. (a),(b) and (c) The zonal variations of the α, $\partial\theta_{es}/\partial z$ and wind shear dV/dz for the continuous clouds over the TP; (d), (e) and (f) The zonal variations of the α, $\partial\theta_{es}/\partial z$ and dV/dz for the continuous clouds at given layer distances (red: 2km; black: 3km).

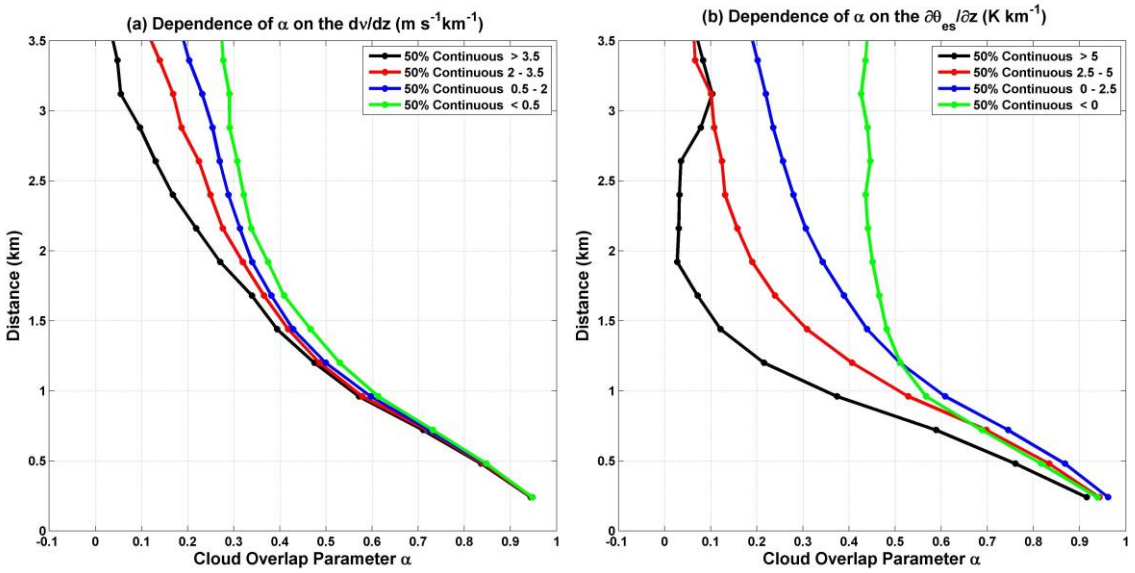

Figure 5. The variation of overlap parameter α with layer distance under different large-scale dynamics. (a): wind shear and (b): instability.

880

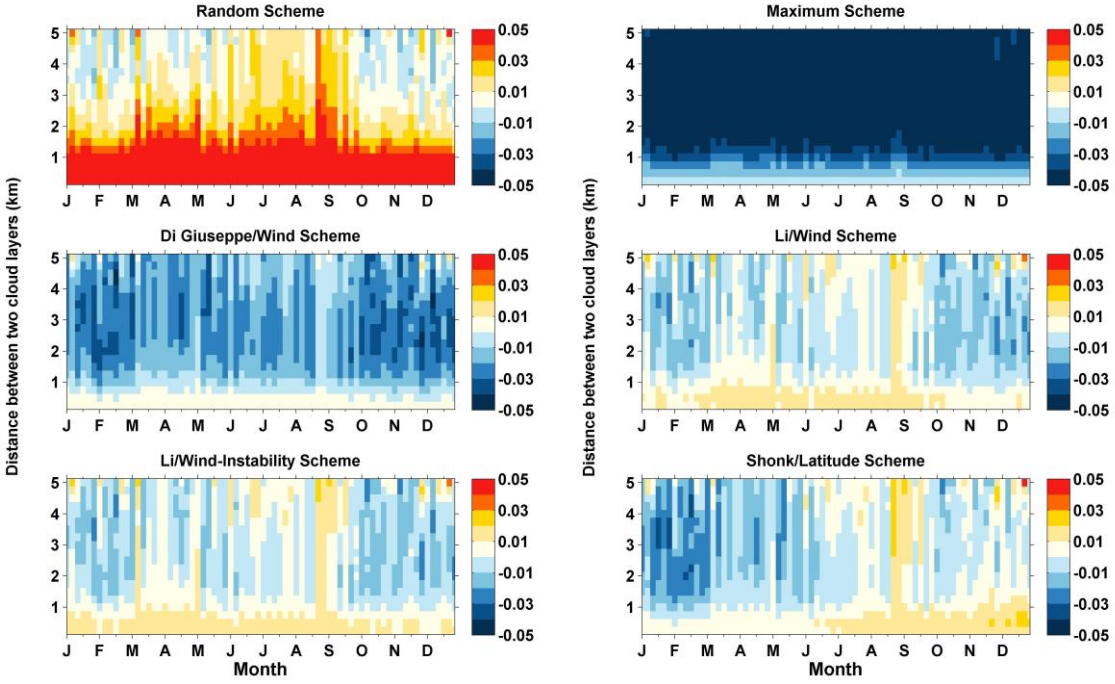

Figure 6. The monthly difference of cloud cover between calculated and observed for different schemes (see the Table 1) and its variation with layer distance.

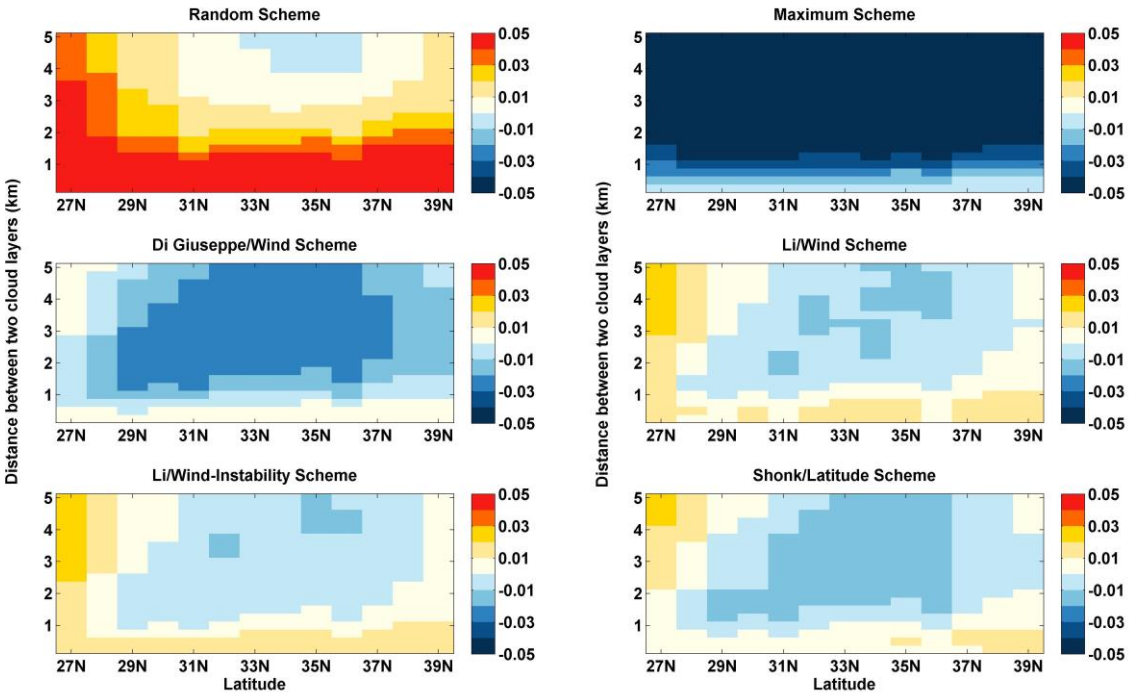

Figure 7. The zonal difference of cloud cover between calculated and observed for different schemes (see the Table 1) and its variation with layer distance.